The Effect of Sigma Phase Formation on the Corrosion and Mechanical Properties of Nb-Stabilized Stainless Steel Cladding

Increases in sigma phase content are found to enhance hydrogen embrittlement, reduce impact toughness, and increase crack growth rates

BY K. KLEMETTI, H. HÄNNINEN, AND J. KIVILAHTI

ABSTRACT. The delta ferrite in a Nb-stabilized austenitic cladding decomposes during stress relief heat treatments (10 to 600 h at 670° C, or 1238°F,) forming sigma phase and secondary austenite. Tensile, impact, and crack opening displacement tests revealed the embrittling effect of the sigma phase.

As little as 3% of sigma phase reduced the impact toughness at room temperature more than 50%. The precipitation of sigma phase was not found to have any significant effect on the anodic polarization behavior of the test material. The austenite matrix dissolved more easily than the delta ferrite and sigma phases during the anodic polarization. The effect was opposite in the electrochemical potentiokinetic reactivation tests where the delta ferrite and sigma phase networks were selectively dissolved.

Slow strain-rate tests did not cause stress corrosion cracking in hot 0.58N H_3BO_3 solution. In 1N HCl solution the cracks grew as the delta ferrite and sigma phases were selectively dissolved. The crack growth rate increased with increasing sigma phase content. Hydrogen charging embrittled the material markedly, and this effect was enhanced by an increase in sigma phase content.

Introduction

Austenitic stainless steel surfacing is commonly used to protect ferritic pressure vessels from the corrosive environment in nuclear reactors and chemical process plants. The chemical composition of the weld metal and the welding conditions are often chosen such that a duplex austenitic-ferritic microstructure is achieved, because it has been shown that small amounts of delta ferrite (5 – 10%) effectively prevent hot-cracking (Ref. 1). On the other hand, recent studies (Refs. 2, 3) have shown that the mode of solidification is more important than the amount of retained delta ferrite in determining the sensitivity to hot cracking; stainless steels, which solidify as primary delta ferrite, are more resistant than those in which austenite is the primary phase. When exposed to elevated temperatures (500 to 900°C, *i.e.*, 932 to 1652°F), the delta ferrite can decompose and produce sigma phase, which has some deleterious effects on the properties of the cladding.

Sigma phase is a hard and brittle intermetallic compound, consisting mainly of Fe and Cr in stainless steels. Sigma phase and its properties have been reviewed by Hall and Algie (Ref. 4). Sigma phase precipitates more easily in delta ferrite than in austenite, because during solidification delta ferrite has been enriched in Cr. Other elements, which promote the tendency to form sigma phase, are Mo, Si, V and Nb (Ref. 5). In recent studies using Mössbauer effect measurements, delta ferrite has been found to transform into about 70% of sigma phase and about 30% of secondary austenite, with the greatest transformation rate occuring at 750°C, *i.e.*, 1382°F (Ref. 5).

The impact toughness of the weld metal is markedly reduced when sigma phase is present (Refs. 6, 7). The embrittling effect of sigma phase depends on its amount and distribution. In weld metals the distribution of sigma phase is inherited from the distribution of delta ferrite. Networks containing more than 6% of delta ferrite have been observed to produce continuous sigma networks during complete decomposition (Ref. 8).

The effect of sigma phase on corrosion resistance is not clear. Albritton and Kadlecek (Ref. 9) stated that sigma phase does not have a marked effect on corrosion resistance. The opposite observation has been introduced by Daemen and Dept (Ref. 10), who propose that the electrochemical potential difference between sigma phase and austenite causes local corrosion. Brouwer (Ref. 11) suggested that sigma phase causes local Cr-depleted zones in austenite, but this probably is not the case concerning weld metals where sigma phase has precipitated in delta ferrite enriched in Cr during solidification (Refs. 12, 13). According to Takalo *et al* (Ref. 14) sigma phase corrodes only in the transpassive region when the environment is heavily oxidizing. The effect of sigma phase on stress corrosion cracking has not been studied. However, Watanabe *et al.* (Ref. 15) observed that hydrogen in weld metals containing sigma phase reduced the elongation markedly.

The aim of this work was to study the tendency of a Type 347 stainless steel cladding to form sigma phase during stress relief heat treatments and the effect of the sigma phase on mechanical and corrosion properties of the cladding

K. KLEMETTI and H. HÄNNINEN are with the Technical Research Centre of Finland, and J. KIVILAHTI is with the Helsinki University of Technology in Finland.

Table 1—Chemical Compositions of the Cladding Layers after Welding, Wt-%

Layer	C	Si	Mn	Cr	Ni	Mo	Nb	P	S	N
1st	0.043	1.06	1.03	20.3	10.2	0.14	0.48	0.011	0.008	0.045
2nd	0.023	1.13	0.97	19.4	10.3	0.10	0.51	0.011	0.011	0.055
3rd	0.021	1.16	0.92	19.4	10.3	0.09	0.51	0.011	0.011	0.058

material.

Experimental Methods

Materials and Heat Treatments

The test material was Nb-stabilized austenitic stainless cladding welded on 120 mm (4.72 in.) thick ASTM AS33 B type pressure vessel steel using submerged arc strip welding. The cladding was 10 mm (0.39 in.) thick and consisted of three layers. The chemical compositions of the different layers after welding are given in Table 1. The 10 mm (0.39 in.) thick cladding was cut off the base material, and three specimens were heat treated as shown in Table 2.

Ferrite contents were measured with a permeability meter (Fischer Ferritescope FE) and sigma contents by using a point count technique. Sigma phase was identified by transmission electron microscopy (TEM).

Table 2—Heat Treatments of the Test Materials

Material	Heat treatments[a]
A	As-welded
B	Stress relieved 14h at 615°C + 10h at 670°C
C	Stress relieved 14h at 615°C + 42h at 670°C
D	Stress relieved 14h at 615°C + 600h at 670°C

(a) °F = 9/5°C +32

Mechanical Properties

Tensile tests were performed for two specimens of each material. The size and the orientations of the tensile test specimens are shown in Fig. 1.

Charpy V-notch impact tests were performed in the temperature range −196 to 600°C (−319 to 1112°F) using a 14.7 J hammer. Because the cladding was too thin for standard specimens, the dimensions of the test specimens were obtained by multiplying the standard dimensions by a factor of 0.6. The specimens were taken perpendicular to the welding direction, and the length of the notch was parallel to the surface of the cladding.

COD (crack opening displacement) tests were performed for materials B, C and D according to the standard BS 5762: 1979 (Ref. 16). The specimens (Fig. 2) had to be made smaller than the standard required. The orientations were the same as those of impact specimens.

Corrosion Tests

The effects of phase transformations on corrosion resistance were studied by measuring anodic polarization curves in de-aerated 1N H_2SO_4 solution at room temperature. The polarization speed was 20 mV/min. The specimens were polished with 1 μm (0.00004 in.) diamond paste before the measurement.

The electrochemical potentiokinetic reactivation test (EPR) was applied to detect sensitization. The method is based on measuring the activation charge while the potential of the specimen is swept from the passive region to the active region (Ref. 17-19). In this test the electrolyte was de-aerated 1N H_2SO_4 solution containing 0.01 M NH_4SCN as an anodic activator. The specimens were polished with 1 μm (0.00004 in.) diamond paste and etched for 30 seconds (s) in aqua regia before testing. This method has been found to reduce pitting attack (Ref. 20). The specimens were passivated at 200 mV_{SCE} for 2 minutes (min), and after that the potential was swept at a scan rate of 100 mV/min to the rest potential while the current density was recorded. The tests were performed at room temperature. Microscopic examination of the specimens revealed the corrosion attack morphology.

The susceptibility to stress corrosion cracking (SCC) was studied by using slow strain-rate tests (SSRT). The specimens shown in Fig. 3A were tensile tested in an electrolytic cell (Fig. 3B) at constant strain rate (5.4×10^{-7} s^{-1}). Two electrolytes were used: 1N HCl solution at room temperature and 0.58N H_3BO_3 solution at 80°C (176°F). The latter was chosen because it simulates the environment of a pressurized water reactor (PWR) during shutdowns.

The effect of hydrogen was studied by charging 0.2 mm (0.008 in.) thick tensile specimens with hydrogen through cathodic polarization. The method is described in detail elsewhere (Ref. 21). The charging was performed at room temperature in a 1N H_2SO_4 solution containing 0.25 g $NaAsO_2$/1. The current

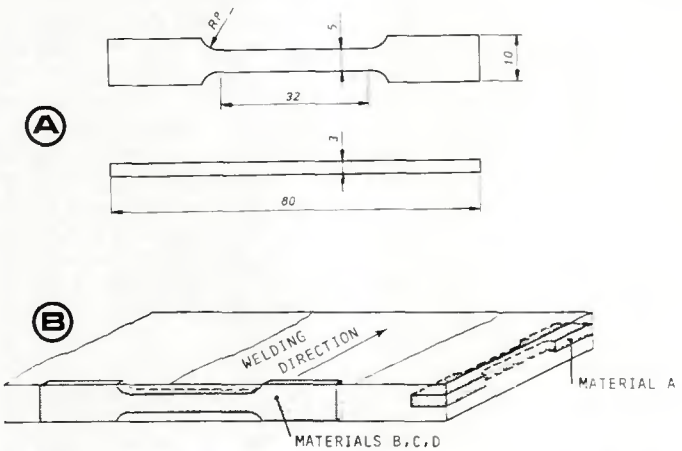

Fig. 1—Tensile test specimen: A—dimensions (mm); B—orientations in the cladding

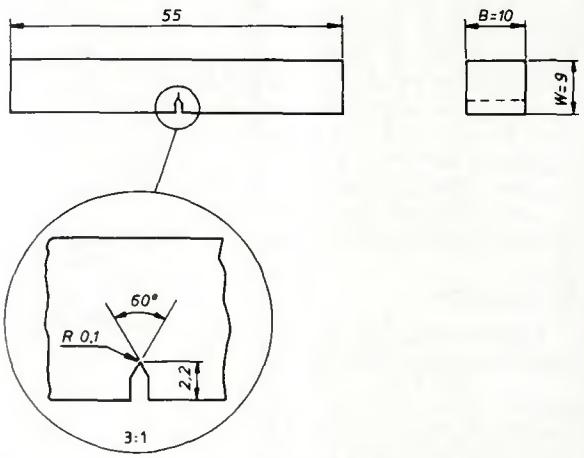

Fig. 2—Crack opening displacement (COD) test specimen

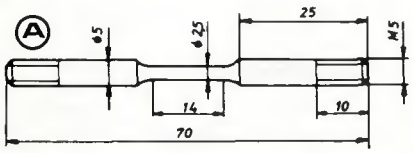

Fig. 3—Slow strain rate test (SSRT) for stress corrosion cracking (SCC) studies: A—test specimen; B (right)—test cell

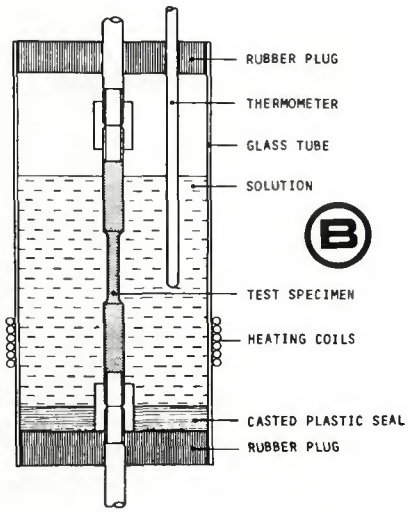

density was 50 mA/cm,^{2} and the charging times varied from 6 to 24 h. The specimens were tensile tested at a crosshead speed of 50 mm/min (2 ikm) within 5 min of charging.

Results of Microscopic Examination and Mechanical Testing

Microstructure

The phase contents of the test materials are shown in Table 3. The ferrite content is the average of several Ferritescope readings, and the sigma content was measured by using a point count technique. These results show that delta ferrite has decomposed and produced sigma phase during stress relief heat treatments. Even the shortest treatment (14 h at 615°C + 10 h at 670°C or 14 h at 1139°F + 10 h at 1238°F) has produced about 1% sigma phase.

Table 3 reveals that, in addition to sigma, some other non-magnetic phases must have been produced during the decomposition; this supports the idea that secondary austenite is also formed.

Table 3—Delta Ferrite and Sigma Phase Contents of the Test Materials, Vol – %

Material	Ferrite	Sigma
A	9	0
B	6	1
C	4	3
D	<1	6

TEM observations of material D (Fig. 4) showed carbide- and dislocation-free areas which often cracked during examination. The electron diffraction pattern of this phase (Fig. 4C) proved it to be sigma phase. The austenite matrix contained small precipitates (Fig. 4D) which based on size, shape and distribution are probably niobium carbonitrides.

The difference in the morphology between delta ferrite and sigma phase can be seen in Fig. 5. According to DeLong (Ref. 22), 4 to 7% of delta ferrite can form continuous networks. This can

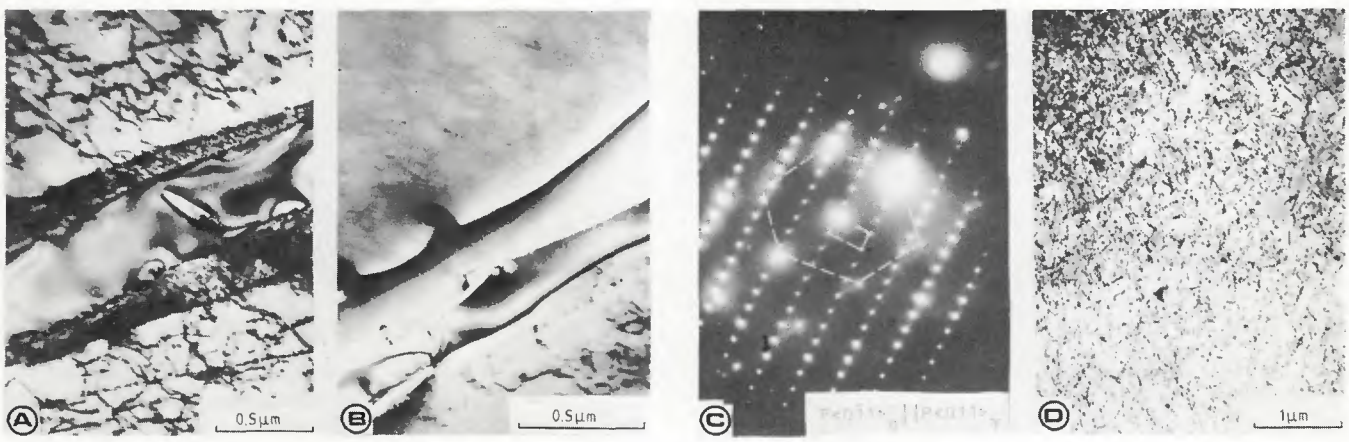

Fig. 4—Transmission electron microscope (TEM) micrographs of material D: A—sigma phase in austenite; B—cracked sigma phase; C—diffraction pattern of sigma phase; D—Nb (CN) precipitates in austenite

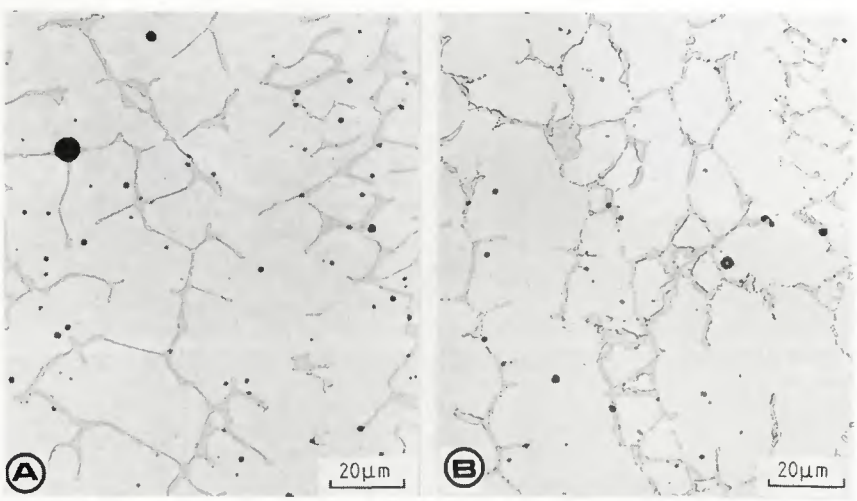

Fig. 5—Morphology difference between delta ferrite and sigma phase: A—delta ferrite network in material A; B—sigma phase in material D. Electrolytic NaOH etching

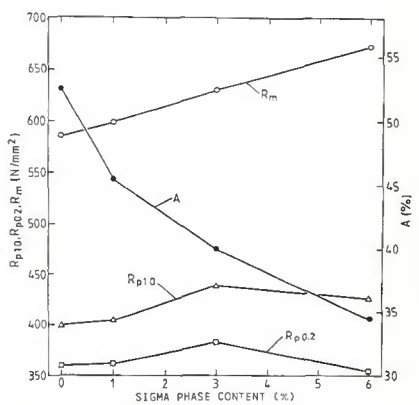

Fig. 6—Tensile test results as a function of sigma phase content

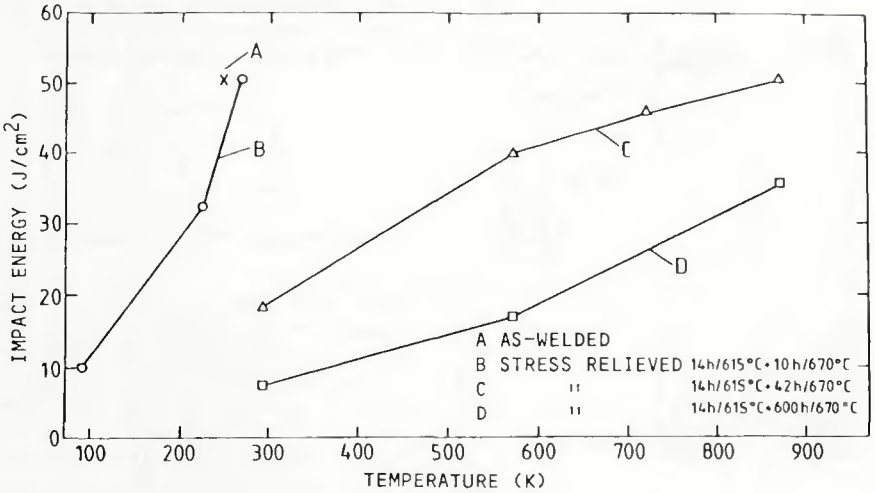

Fig. 7—Charpy V-notch impact energies as a function of temperature

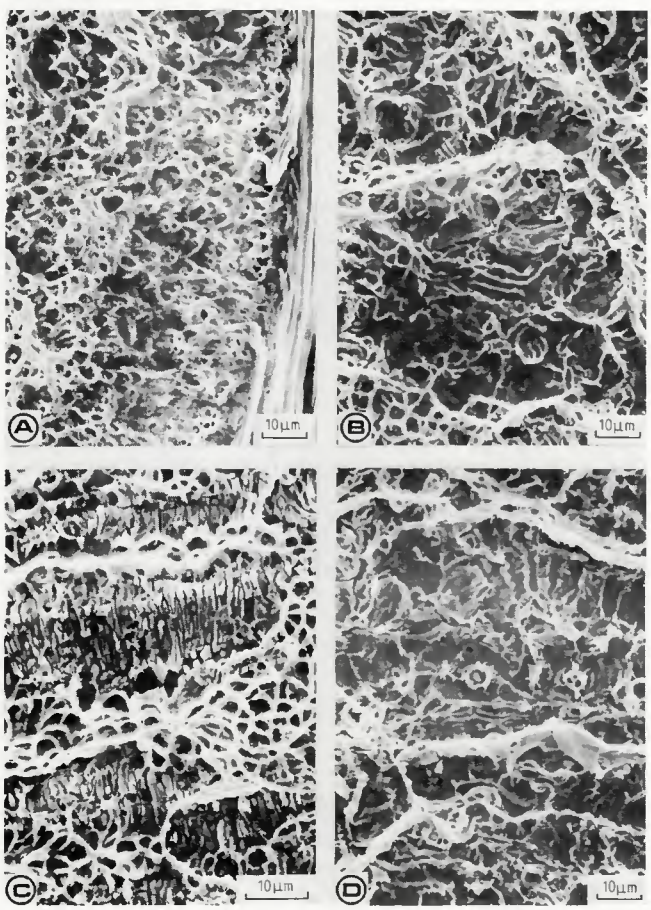

Fig. 8—Fracture surfaces of impact specimens tested at room temperature: A—material A, impact energy > 50J/cm²; B—material B, impact energy > 50 J/cm²; C—material C, impact energy = 18 J/cm²; D—material D, impact energy = 7.5 J/cm² (note: J/cm² ÷ 6.452 = J/in.²)

be confirmed on the basis of Fig. 5.

Mechanical Properties

The effects of sigma phase content on the tensile test properties are presented in Fig. 6. As the sigma phase content increases, the tensile strength increases while elongation to fracture decreases, *i.e.*, the material becomes more brittle. The small effect on yield strengths can be explained through Nb(C, N) precipitation in the matrix.

Figure 7 shows the impact energies in J/cm² (equal to J/in.² after dividing by 6.452) of the miniature test specimens. Material A was too tough for the small hammer used in these tests. However, the embrittling effect of sigma phase is evident. At room temperature the specimens containing more than 3% sigma phase were brittle. The toughness increased to some degree as the testing temperature increased. The fracture surfaces of the impact specimens tested at room temperature are shown in Fig. 8. As the sigma phase content increases, the fraction of tough micro-void coalescence type fracture decreases. In material D (Fig. 8D) most of the fracture is planar.

The force-displacement curves measured in COD tests are presented in Fig. 9. The values obtained from the tests and the calculated crack openings (δ_c) are presented in Table 4. The crack opening decreases as the sigma phase content increases, and the embrittling effect of sigma phase can also be deduced on the basis of the curves in Fig. 9.

Corrosion Tests

Anodic Polarization Curves

The anodic polarization curves obtained were typical of stainless steels, and no significant variations between different heat treatments could be detected. SEM examinations revealed that during anodic polarization the austenite matrix had dissolved more than the delta ferrite (Fig. 10A) or sigma phase (Fig. 10B) networks. The attack on the matrix was strongest at the phase boundaries, and the matrix was also dissolved around inclusions. On the basis of Fig. 10B it is obvious that the secondary austenite formed during the decomposition of del-

Table 4—Crack Opening Displacement (COD) Test Results[a]

Material	a, mm	a/W	Y	P, N	V_c, mm	V_p, mm	σ_y, N/mm²	K, N/mm$^{3/2}$	δ_c, mm
B	5.823	0.647	18.1	2480	0.76	0.61	362	1496	0.103
C	5.596	0.622	16.4	2360	0.21	0.09	384	1290	0.024
D	5.847	0.650	18.3	1800	0.15	0.04	352	1098	0.013

(a) 1 in. = 25.4 mm; N/mm² ÷ 6.894757 = ksi.

ta ferrite dissolves, leaving cavities in the sigma phase network.

Intergranular Corrosion Tests

Based on EPR test results, intergranular corrosion was not detected in any material. As Fig. 11 shows, the delta ferrite and sigma phase networks were attacked during the tests. Some pits can be seen in the austenite matrix, probably due to attack on inclusions. The activation charges of materials A, B and C were almost the same, while the charge of material D was about six times greater. This suggests that sigma phase is more easily dissolved than delta ferrite.

Stress Corrosion Cracking Tests

The stress-strain curves obtained in slow strain-rate SCC tests are shown in Fig. 12. In hot 0.58N H_3BO_3 solution, the tensile strengths and the elongations to fracture were only slightly smaller than those measured in normal tensile tests. In 1N HCl solution the elongations to fracture were markedly reduced, and the tensile strengths were about 100 N/mm^2 (14.504 psi) smaller than in H_3BO_3 solution.

The effect of sigma phase on specimens tested in boric acid was similar to those tested in air (normal tensile tests). The inconsistency between the samples A and B (Fig. 12A) may be due to inaccuracy in the testing procedure. The SEM examination of fracture surfaces showed only micro-void coalescence type of fracture, although the voids became smaller and flatter when the sigma phase content increased.

The SSRT results in HCl (Fig. 12B) showed that sigma phase had a stronger effect on elongation to fracture than in normal tensile tests. A cellular dendritic solidification structure is clearly visible in the SEM-micrographs of the fracture surfaces of material A (Fig. 13), and a small ductile fracture area can be seen in the center of the fracture surface. In some areas the fracture has propagated transgranularly (marked with T in Fig. 13B); this may be due to the discontinuity of the ferrite network. When the sigma phase content increased, the fraction of ductile fracture decreased. In material D the fracture has propagated along the delta ferrite-sigma network through the whole test specimen—Fig. 14.

Microsections through SSRT specimens A and D are shown in Fig. 15. Specimen A has a number of cracks on its surface, and the delta ferrite is selectively dissolved (Fig. 15A) while the specimen containing sigma phase (D in Fig. 15B) has only one main crack. This crack has probably propagated so fast that the surface of the specimen has not had time to dissolve as much as in material A.

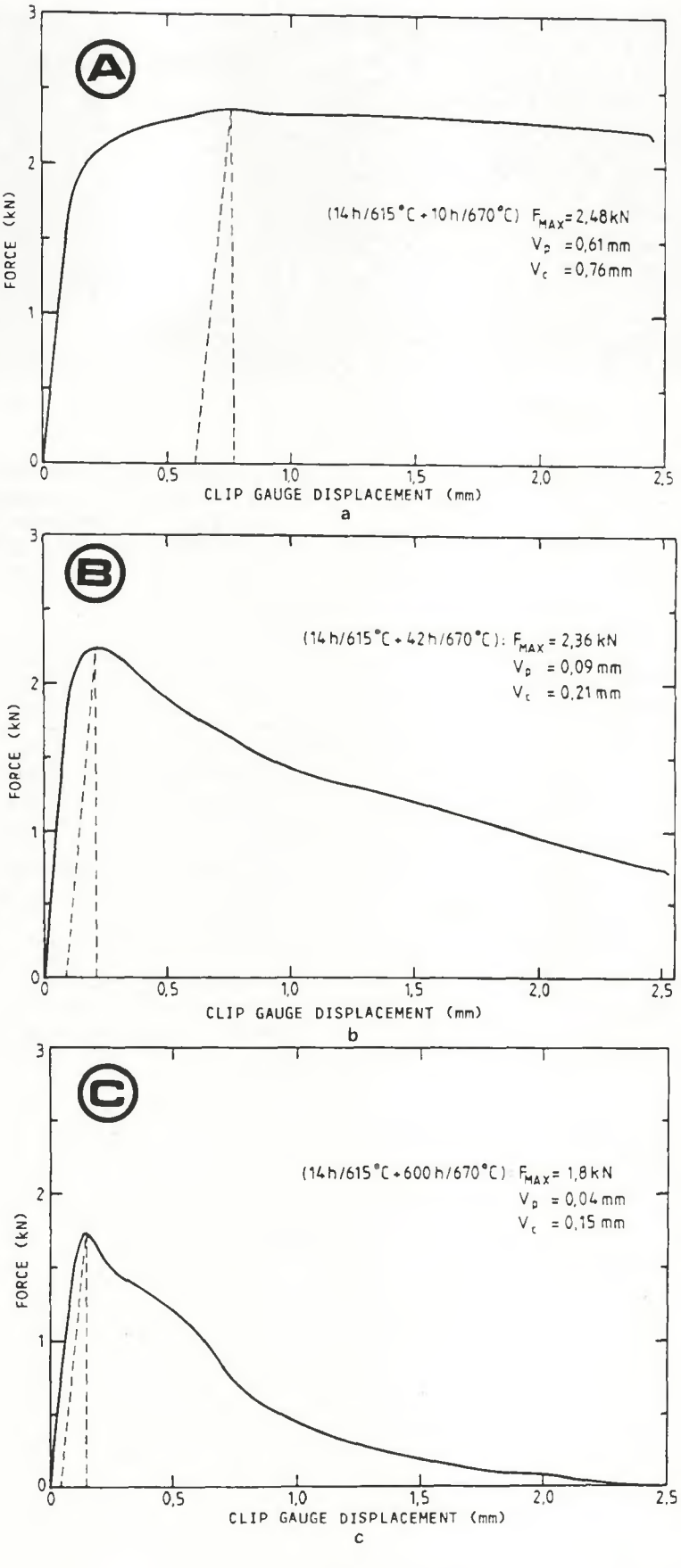

Fig. 9—Force-clip gauge displacement curves: A—material B, B—material C; C—material D

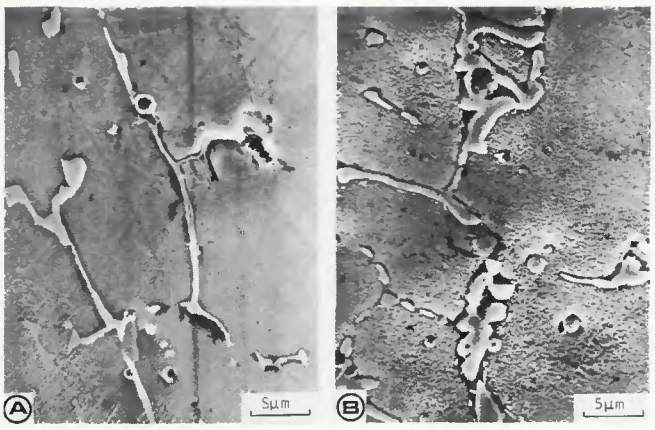

Fig. 10—Microstructures after anodic polarization tests in 1N H_2SO_4 solution at room temperature: A—material A; B—material D

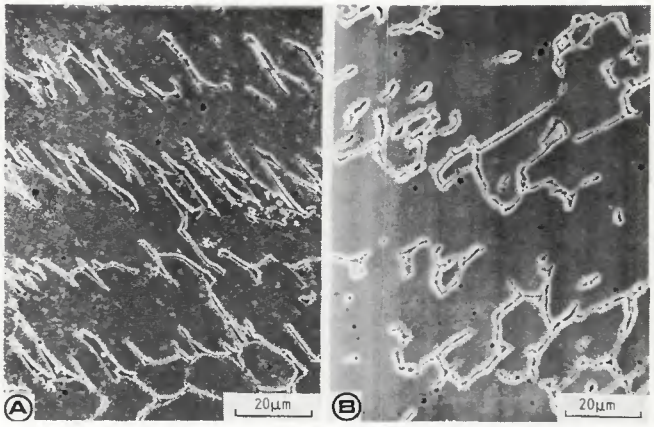

Fig. 11—Microstructures after electrochemical potentiokinetic reactivation (EPR) test: A—material A; B—material D

Hydrogen Embrittlement Tests

Hydrogen charging reduced the elongation to fracture significantly. The elongations ranged from 4 to 6%, and the highest sigma phase content gave the lowest values. The tensile strengths were also reduced when hydrogen was present. Figure 16 shows that the reduction of tensile strengths increased as the sigma phase content increased, while in normal tensile tests the effect was the opposite.

A narrow (about 30 μm, *i.e.*, equivalent to 0.0012 in.) cleavage fracture zone could be seen at the edge of the fracture surfaces—Fig. 17. Cracks on the surfaces of the specimens are shown in Fig. 18. In material containing sigma phase (Fig. 18B), most of the cracks have propagated along the sigma phase networks which seem to have dissolved a little during the cathodic polarization. The fracture path in material containing only delta ferrite (Fig. 18A) is not clearly distinguishable.

Charging time did not seem to have any marked effect on the fracture behavior. This was unexpected since delta ferrite and sigma phase boundaries should have operated as short-circuit paths for hydrogen diffusion.

Discussion

According to the chemical analysis of the welded material, the weldment has solidified primarily as delta ferrite; also, because of the fast cooling rate, the ferrite has remained stable at the axes of the cellular dendrites (Ref. 23). In spite of the heat input generated by the welding of subsequent layers, no sigma phase was detected in the as-welded condition. On the other hand, during stress relief heat treatments at 670°C (1238°F), delta ferrite has decomposed to sigma phase and secondary austenite.

Because of the low carbon content and Nb-stabilization, only small Nb (C, N) particles have precipitated in the austenite matrix and no sensitization can be detected in the EPR tests. The possible diffusion of carbon from the ferritic base material to the cladding during stress relief heat treatment could not be studied, because the cladding had been cut off before heat treatments; this is not the situation in practice.

Based on the results of the tensile tests, the brittleness caused by sigma phase is not deleterious to the cladding. This is because, even after the longest heat treatment (600 h at 670°C, *i.e.*, 1238°F), the elongation to fracture was still as much as 30%. However, only 3% of sigma phase reduces the Charpy V-notch impact toughness more than 50%. It is obvious that the fracture has propagated through the sigma phase or along the phase boundaries of the delta ferrite-sigma networks, since the fraction of brittle fracture increases with increasing sigma content. COD tests also showed that sigma phase has a strong embrittling effect.

Stress relief heat treatments did not affect the polarization behavior of the test material. The austenite matrix proba-

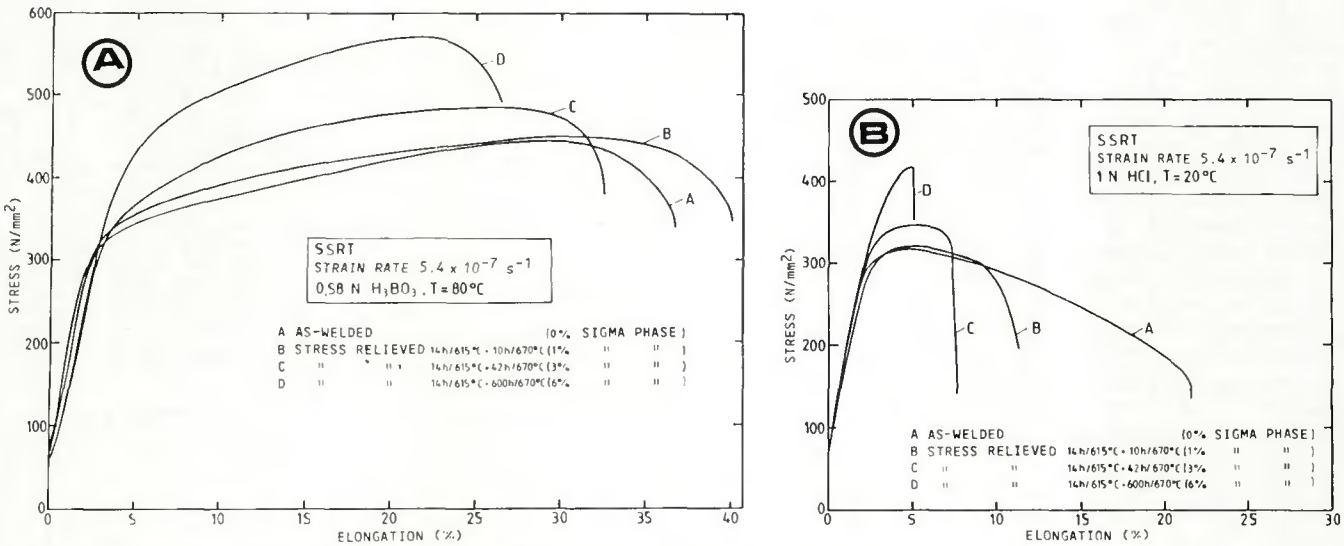

Fig. 12—Stress-strain curves (SSRT) measured in two different solutions: A—0.5BN H_3BO_3; B—1N HCl

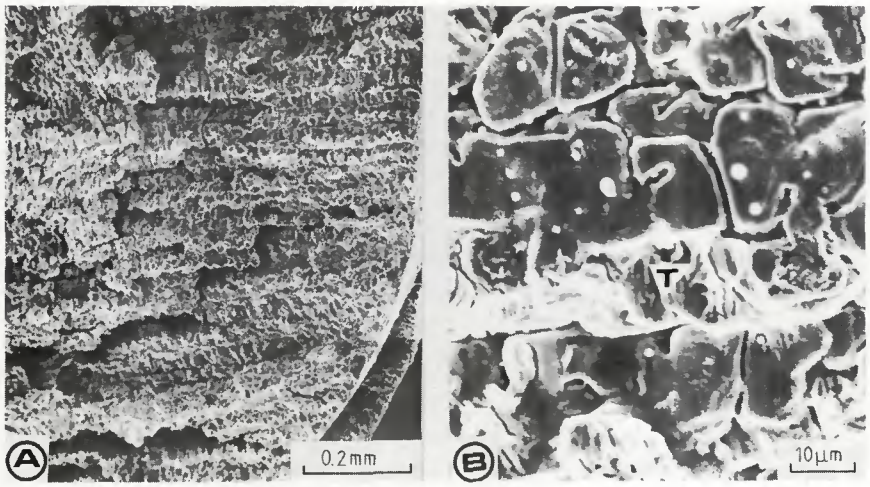

Fig. 13—Scanning electron microscope (SEM) micrographs of SSRT specimen A tested in 1N HCl solution

bly dissolved in the active state more easily than the delta ferrite and sigma phases, thus revealing these phases. Because of the different electrochemical properties of these phases, the dissolution has been more severe at the phase boundaries.

EPR tests showed that delta ferrite and, in particular, sigma phase were selectively dissolved at potentials below 200 mV. The reason why these phases were not passivated is not clear. In fact, considering their high Cr content, they are expected to be more passive than the austenite matrix.

Slow strain-rate tests did not cause stress corrosion cracking in hot 0.58N H_3BO_3 solution. In 1N HCl solution, the cracks grew as the delta ferrite and sigma phases were selectively dissolved. The discontinuity of the delta ferrite-sigma network caused regions of transgranular SCC in the austenite. This observation is supported by the results of Baeslack *et al* (Ref. 24), who studied austenitic stainless weld metals containing delta ferrite only. In our tests sigma phase increased the crack growth rate. On the basis of the different fracture morphology compared to hydrogen induced cracking, it can be deduced that the SCC growth mechanism in HCl solution is controlled by selective dissolution of delta ferrite and/or sigma phase, and not by cathodic hydrogen evolution and subsequent hydrogen embrittlement.

Hydrogen embrittles the cladding

Fig. 14—Fracture surface of SSRT specimen D tested in 1N HCl solution

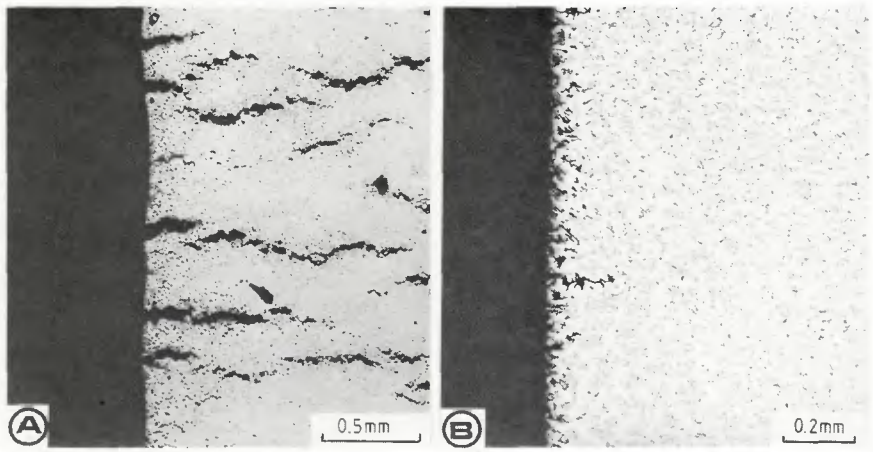

Fig. 15—Microsections through SSRT specimens tested in 1N HCl solution: A—specimen A; B—specimen D. Electrochemical etching in NaOH solution

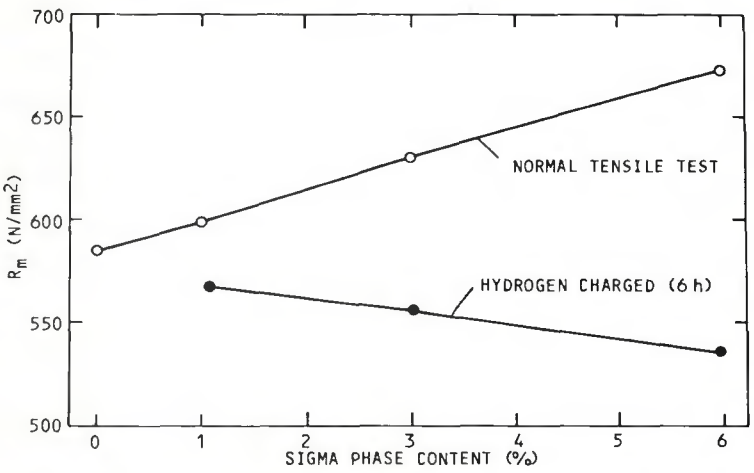

Fig. 16—Effect of hydrogen charging (time 6 h) on tensile strength as a function of sigma phase content

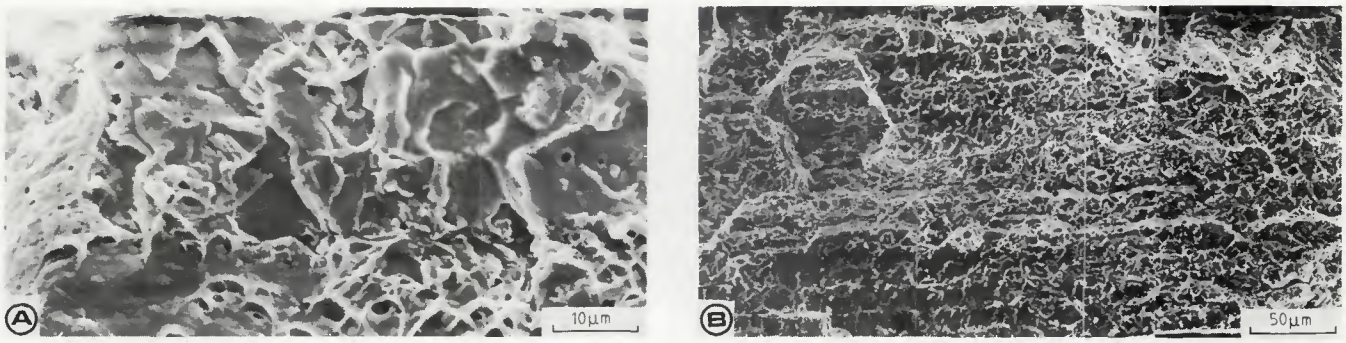

Fig. 17 — Fracture surfaces of hydrogen charged specimens: A — cleavage fracture zone at the edge of specimen A (charging time 17.5 h); B — fracture surface of material D (charging time 24 h)

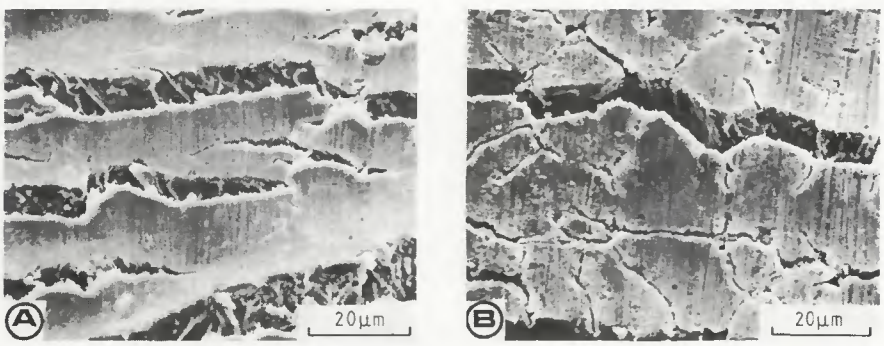

Fig. 18 — Cracks on the surfaces of hydrogen charged specimens: A — material A; B — material D

material markedly. Elongations to fracture were only about a tenth of the original values when hydrogen was present in the metal. Brooks and West (Ref. 25) have observed that cracks in hydrogen charged specimens grow along the delta ferrite-austenite phase boundaries. The hydrogen-induced fracture zones observed in these tests have probably formed both interdendritically and transgranularly. It is evident that low cycle fatigue caused by startups and shutdowns of the plant may cause cracking in cladding material containing sigma phase, particularly when the environment contains hydrogen.

Conclusions

On the basis of the results obtained in this work the following conclusions can be made:

1. Sigma phase precipitates during stress relief heat treatments in 20Cr/10Ni-type austenitic stainless weld metals containing delta ferrite.

2. Delta ferrite decomposes to sigma phase and secondary austenite; long heat treatments (600 h at 670°, *i.e.*, 1238°F) transformed about two-thirds of the delta ferrite into sigma phase.

3. Sigma phase embrittles the weld metal markedly; as little as 3% of sigma phase may reduce the impact toughness to one half of the original value.

4. The presence of sigma phase had no effect on the anodic polarization behavior of the material.

5. Both delta ferrite and sigma phase were selectively dissolved during the EPR (electrochemical potentiokinetic reactivation) test.

6. Selective dissolution of delta ferrite and sigma phase occurs in slow strain-rate tests performed in 1N HCl solution, and an increasing sigma phase content increases the crack growth rate.

7. SSRT (slow strain rate tests) in hot 0.58N H_3BO_3 solution did not produce SCC (stress corrosion cracking).

8. Hydrogen embrittles the cladding material significantly, and an increase in sigma phase content enhances the embrittlement.

Acknowledgments

The work discussed in this paper was performed at the Technical Research Centre of Finland as a part of the Reliability of Reactor Materials Program financed by the Ministry of Trade and Industry of Finland. Imatran Voima Oy is acknowledged for providing the test material.

References

1. Hull, F. C. 1967. Effect of delta ferrite on the hot cracking of stainless steel. *Welding Journal* 46(9):399-s to 409-s.

2. Takalo, T., Suutala, N., and Moisio, T. 1979. Austenitic solidification mode in austenitic stainless steel welds. *Metallurgical Transactions* 10A:1173-1181.

3. Cieslak, M. J., and Savage, W. F. 1981. Technical note: ferrite morphology in high molybdenum stainless steels. *Welding Journal* 60(8):131-s to 134-s.

4. Hall, E. O., and Algie, S. H. 1966. The sigma phase. *Metallurgical Reviews* 11:61-88.

5. Wegrzyn, J., and Klimpel, A. 1981. The effect of alloying elements on sigma phase formation in 18-8 weld metals. *Welding Journal* 60(8):146-s to 154-s.

6. Talbot, A. M., and Furman, D. E. 1953. Sigma formation and its effect on the impact properties of iron-nickel-chromium alloys. *Trans. ASM* 45:429-442.

7. Creamer, E. L., Rozalsky, I., and Leonard, R. W. 1969. Embrittlement of Type 347 stainless steel weldments by sigma phase. *Welding Journal* 48(6):239-s to 244-s.

8. Spruiell, J. E., Fett, W. E., and Lundin, C. D. 1977. Technical note: ferrite stability at elevated temperature in austenitic stainless steel weld metal. *Welding Journal* 56(9):289-s to 290-s.

9. Albritton, O. W., and Kadlecek, P. E. 1968. Microstructural variations in welded austenitic stainless steel caused by heating at 1350°F. *Welding Journal* 47(2):73-s to 81-s.

10. Daemen, R. A., and Dept, F. 1970. Submerged-arc stainless steel strip cladding. *Welding Journal* 49(1):33-s to 40-s.

11. Brouwer, G. 1971. Ferrite in austenitic stainless steel weld metal and its consequences. *Aust. Welding Journal* 15(7):76-83.

12. Castro, R. J., and deCadenet, J. J. 1975. *Welding metallurgy of stainless and heat-resisting steels.* London: Cambridge University Press.

13. Pinnow, K. E., and Moskowitz, A. 1970. Corrosion resistance of stainless steel weldments. *Welding Journal* 49 (6):278-s to 283-s.

14. Takalo, T., Karjalainen, P., and Moisio, T. 1974. δ-ferriitin vaikutus austeniittisten ruostumattomien terästen hitsiaineen korroosioon. *Kemia* 1(2):89-92.

15. Watanabe, J., Ohnishi, K., Murai, M., and Chiba, R., 1978. On the cracks in stainless steel internal attachment welds for high temperature, high pressure hydrogen services. Corrosion/78, paper no. 104, San Francisco, California, March 14-18, 1978.

16. British Standard 5762. 1979. *Methods for crack opening displacement (COD) testing.*

17. Clarke, W. L., Cowan, R. L., and Walker, W. L. *Comparative methods for measuring degree of sensitization in stainless steels.* ASTM STP 656, pp. 99-132. Philadelphia: American Society for Testing and Materials.

18. Backman, J., and Purra, T. 1978. Evaluation of the susceptibility to intergranular corro-

sion of stainless steels by a potentiokinetic reactivation method. 8th Scandinavian Corrosion Congress, Helsinki. *Proceedings*, vol. I, pp. 1-8.

19. Aho-Mantila, I., Aaltonen, P., and Hänninen, H. 1981. *Intergranular corrosion testing of austenitic stainless steels.* VTT Research Report 26/1981, Espoo, Finland.

20. Aaltonen, P. 1981. Personal communication.

21. Hänninen, H., and Hakkarainen, T. Fractographic characteristics of a hydrogen charged AISI 316 Type austenitic stainless steel. *Metallurgical Transactions* 10A (8): 1196-1199.

22. DeLong, W. T. 1974. Ferrite in austenitic stainless steel weld metal. *Welding Journal* 53 (7): 273-s to 286-s.

23. Suutala, N., Takalo, T., and Moisio, T. 1980. Ferritic-austenitic solidification mode in austenitic stainless steel welds. *Metallurgical Transactions* 11A:717-725.

24. Baeslack, W. A., Duquette, D. J., and Savage, W. F. 1979. The effect of ferrite content on stress corrosion cracking in duplex stainless steel weld metals at room temperature. *Corrosion* 35 (2):45-54.

25. Brooks, J. A., and West, A. J. 1978 (June). *Hydrogen induced ductility losses in austenitic stainless steel welds.* SAND 78-8675, Sandia Laboratories.

WRC Bulletin 279
July, 1982

Weldability and Fracture Toughness of Quenched and Tempered 9% Nickel Steel: Part I—Weld Simulation Testing
by A. Dhooge, W. Provost and A. Vinckier

An investigation on the weldability of a quenched and tempered 9% Ni steel using weld simulation and artificial aging to estimate the heat-affected zone ductility at cryogenic temperatures is reported in Part I. Charpy-V bars were subjected to various weld simulation cycles and subsequent heat treatments and, after notching, broken at a range of cryogenic temperatures.

Weldability and Fracture Toughness of Quenched and Tempered 9% Nickel Steel: Part II—Wide Plate Testing
by A. Dhooge, W. Provost and A. Vinckier

In addition to standard impact and tensile tests, a large number of wide plate specimens welded with various consumables and welding processes were tested to evaluate the toughness and defect acceptability of 9% Ni steel in plate thicknesses greater than 25 mm.

Publication of these reports was sponsored by the Weldability Committee of the Welding Research Council.

The price of WRC Bulletin 279 is $10.00 per copy, plus $3.00 for postage and handling. Orders should be sent with payment to the Welding Research Council, 345 East 47th St., New York, NY 10017.

WRC Bulletin 281
October, 1982

Hydrodynamic Response of Fluid Coupled Cylinders, Simplified Damping and Inertia Coefficients
by S. J. Brown

This study presents the development of the concept of inertia and damping coefficients in an historical context with experimental, classical and numerical investigations into the dynamics of fluid coupled cylinders. It is shown that coefficients may be used to account for coaxial cylinder end conditions, eccentricity, skewness, clusters, shell modes and axial modes.

Publication of this report was sponsored by the Subcommittee on Dynamic Analysis of Pressure Components of the Pressure Vessel Research Committee of the Welding Research Council.

The price of WRC Bulletin 281 is $11.50 per copy, plus $3.00 for postage and handling (foreign + $5.00). Orders should be sent with payment to the Welding Research Council, 345 E. 47th St., Room 1301, New York, NY 10017.